Accepted for publication in Journal of Rail and Rapid Transit 7 July 2019.

DOI: 10.1177/0954409719868050

Effect of train speed and track geometry on the ride comfort of high-speed railways based on ISO 2631-1

Chi Liu[1], David Thompson[1], Michael J Griffin[1], Mani Entezami[2]

[1] Institute of Sound and Vibration Research, University of Southampton, Southampton SO17 1BJ, UK

[2] Birmingham Centre for Railway Research and Education, University of Birmingham, Edgbaston, Birmingham, B15 2TT, UK

Corresponding author:

Dr. Chi Liu, Institute of Sound and Vibration Research, University of Southampton, Southampton SO17 1BJ, UK. E-mail: liuchi0511@gmail.com

Abstract

The operational speeds of passenger trains have been increasing and now often exceed 300 km/h. Higher speeds can lead to increased vibration and reduced ride comfort for railway passengers. This study investigates the combined effect of speed and track geometry on vibration discomfort in high-speed trains. Railway vehicle dynamic models with various levels of complexity are used, with the measured geometry of a section of high-speed track as an input. The models have been calibrated with vibration measurements carried out in a train running over this section of track and then applied to predict vibration discomfort at increased speeds. To evaluate the vibration discomfort at speeds up to 400 km/h, information on track geometry should include wavelengths up to at least 150 m. Vertical irregularities have the greatest effect at all speeds but lateral irregularities are also important. Both the vertical and lateral irregularities of high-speed track should be controlled at wavelengths 50-100 m that excite rigid modes of the car body, corresponding to frequencies of typically 1-2 Hz. Additionally, vertical irregularities with wavelengths 5-12 m that excite the fundamental flexible mode of the car body, typically around 10-15 Hz, should also be controlled. The effects of cant, the rates of change of cant, and the radius of vertical curves are also evaluated although they only have a small effect on vibration discomfort.

Keywords: whole-body vibration, ride comfort, high-speed railways, track geometry, vehicle dynamics

1 Introduction

Since the introduction of the Shinkansen in Japan in the 1960s, the speeds of high-speed passenger trains have been increasing steadily, and now often exceed 300 km/h [1]. With increasing speed, the frequency content of a given track irregularity shifts to higher frequencies, whereas the frequency range over which the human body is most sensitive to vibration discomfort does not change. These changes in the frequency content of the excitation, as well as increases in the vibration magnitude, will affect the ride comfort of railway passengers. Requirements for the track geometry for high speeds are expected to differ from those used for conventional speeds, as longer wavelength irregularities become more important.

When a railway vehicle runs along the track, it largely follows the track geometry in both vertical and lateral directions, producing vibration of the car body in all directions. The sensitivities of the human body to vibration in each direction are different (BS 6841:1987[2]; ISO 2631-1:1997[3]) and therefore the relative importance of the different components of track geometry may differ and change with varying speed. Understanding such factors would assist in setting design requirements for track geometry for higher speeds and in the design of future high-speed trains.

For speeds up to 300 km/h, UIC 703[4] recommends limits to the geometry of the horizontal and vertical curves. Limits for horizontal curves are given in terms of cant, cant deficiency, cant excess, rate of cant deficiency at transitions, and rate of cant gradient; those for the vertical curves are given in terms of the quasi-static vertical acceleration. These limits are recommended for track stresses and safety, track maintenance, and ride comfort. European Standard EN 13848-5 sets out track irregularity limits associated with safety for various wavelength ranges up to 70 m and for train speed up to 360 km/h [5]. For example, as immediate action limits, the longitudinal level with wavelength between 25 and 70 m must be less than 18 mm (zero to peak value) for train speeds between 230 and 300 km/h, and less than 16 mm for speeds between 300 and 360 km/h. However, for wavelengths greater than 70 m, no limit is included in the standard. Other standards on the track irregularity limits for high-speed railways in Japan, France, Germany, China as well as those specified in EN 13848-5, were summarised and

compared by Tian et al [6]. In these standards the maximum wavelength for which a limit is given is up to 150 m in the Chinese standards [7-8] for train speeds between 250 km/h and 350 km/h. The effect on ride comfort of wavelengths greater than 150 m for speeds greater than 250 km/h is unclear.

International and British standards provide guidance on the measurement, evaluation and assessment of whole-body vibration with respect to vibration discomfort. BS 6841[2] and ISO 2631-1[3] provide general guidance. Standards for vibration discomfort in railway vehicles include references 9-12. BS 6841[2] and ISO 2631-1[3] include frequency-dependent weightings for the different directions of vibration. They suggest an 'average' method, using the root-mean-square (r.m.s.) or root-mean-quad (r.m.q.) of the whole length of acceleration signals, and a 'dose' method, using the vibration dose value. EN 12299[9] and UIC Code 513[12] suggest a 'statistical' method using the 95th percentile of 60 sequences of 5 seconds r.m.s. acceleration signals to evaluate vibration discomfort (i.e. 5 minutes in total).

Comfort in railway vehicles can be assessed using a variety of methods. Compared with EN 12299 (which is derived from UIC 513), ISO 2631-1 defines a more complete set of measurement positions, based on 12 vibration inputs: three at the floor, six at the seat pan and three at the backrest. EN 12299 defines a 'Standard method' based only on three directions at the floor and a 'Complete method' based on four positions: vertical acceleration at the floor, vertical and lateral at the seat pan and longitudinal at the backrest. On the other hand, EN 12299 requires longer measurements with at least four blocks of 5 minutes. The Sperling Index, as applied in Ref 13, uses only vertical (or lateral) acceleration of the floor. In the present study the method of ISO 2631-1 is used.

According to ISO 2631-1[3], accelerations should be measured at the feet and at the backrest in the three translational axes, at the seat pan in all six axes (three translations and three rotations) for frequencies in the range 0.5-80 Hz. An overall weighted vibration exposure is then derived to reflect the overall discomfort caused by vibration.

To estimate vibration exposure using dynamic models of the railway system, these should include appropriate models of the vehicle, the track, and the contact mechanics between them. Each of these can have different structures or complexity depending on their applications and frequency ranges. Focusing on frequencies below 80 Hz, in the studies of ride comfort or hunting stability of vehicles, more details of the vehicle structures are required than the track (e.g. Refs 14-19). These models often

represent the vehicle as a two- or three-dimensional multi-body system with either a rigid or a flexible car body.

Rigid-body modes of the car body occur at frequencies less than 3 Hz [19-21] and thus vehicle models for ride comfort analysis should include the primary and secondary suspension. The first order bending and torsional modes of the car body usually occur around 10 Hz [13-14, 19-22]. Flexibility of the car body can affect the ride comfort greatly when the first bending mode is lower than 10 Hz [17] and should therefore be included. The number of flexible modes of the car body that should be considered for vibration discomfort has not been well reported. Using a finite element model of a car body, Diana et al.[23] found 33 modes between 5 and 20 Hz, many of which were local modes. An Euler-Bernoulli beam has been used by some authors to represent the vertical bending of the car body [13, 17-19]. Estimated from the beam parameters given by Sun et al.[13], there are three vertical bending modes below 100 Hz, at approximately 12, 33, and 65 Hz.

As well as the vertical dynamics, lateral track irregularities and horizontal curves can cause lateral and rotational vibration of the car body. Howarth and Griffin[24] measured and evaluated vibration in nine positions/axes of a seated passenger during two scheduled rail journeys for ride comfort. The vertical and lateral vibration at the seat and the fore-and-aft vibration at the backrest were found to contribute most to vibration discomfort. Two-dimensional models, such as those presented in Refs 13, 17 and 19 cannot represent the roll, yaw, and lateral motions and a three-dimensional model [21, 22, 11], is needed.

For the track, software packages for railway vehicle dynamics contain models with different levels of complexity. For example, the Universal Mechanism[27] software has a massless model for the track with only force elements intended for frequencies less than 20 Hz, an inertial model with mass-spring-damper systems for frequencies up to 100 Hz, and a flexible model with a beam supported by an elastic foundation for frequencies up to 1000 Hz. Other computer packages have similar options. For a ballasted track, the vertical point receptance generally shows a flat modulus and a phase close to zero for frequencies up to about 80 Hz and a strongly damped resonance typically between about 80 and 100 Hz [28]. This indicates that the track performs predominantly as a spring at frequencies less than 80 Hz. The vibration decays rapidly along the rail in this frequency region, so there a single degree of freedom mass-spring-damper system may therefore be sufficient.

In the vertical direction, the rail irregularity provides a relative displacement input to the wheel/rail contact. However, in the lateral direction the wheelsets are effectively unconstrained on the railhead (except by flange contact) allowing relative displacement in the lateral direction between the wheels and rails, especially during curving. Model complexity for ride analysis has been studied by Graa et al.[29].

This paper presents a study of the vibration experienced by a seated passenger. For a railway vehicle running on a track with known geometry, the overall vibration exposure is evaluated using the methods from ISO 2631-1[3]. The objective of the study is to determine the relative importance of ~~each~~ components of track geometry in different directions and in different wavelength ranges for train speeds up to 400 km/h.

Although the ride comfort will also depend on the dynamics of the vehicle, the influence of varying vehicle parameters is not considered. Other aspects of the dynamic performance of the system, e.g. details of wheel-rail interaction and running safety are also not considered.

The study is based on the measured geometry of a typical section of track of length 5 km from a high-speed line. This is used together with a three-dimensional model of the vehicle dynamic behaviour, which includes flexible modes of the car body. Vibration measurements have been carried out in a train running over the same 5 km section of track. The vehicle parameters have been determined by tuning the model to match the vibration measurements inside the train. The calibrated model is then used to study the relative importance of the different components of track geometry on ride comfort and how these change with increasing train speed.

2 Measurements

2.1 Vibration measurements on a train

Measurements of rail vehicle motion were made by the authors on an in-service passenger train. Results are used for a 5 km section of the journey which the train traversed with a steady speed of about 210 km/h (58 m/s).

Vibration was measured for a seat located over the rear bogie of a powered vehicle (the fifth of the six coaches of the train, see Figure 1a). The car body has a length of 20 m, width of 2.8 m, height of about 2.6 m (from floor to ceiling), and bogie centre distance of 14.2 m. The seat was in Standard Class and

consisted of fabric-covered foam cushions; it was located by the window facing the running direction. During the period of measurement, a subject (height 1.70 m, weight 65 kg) sat in the seat and maintained a typical upright seated posture.

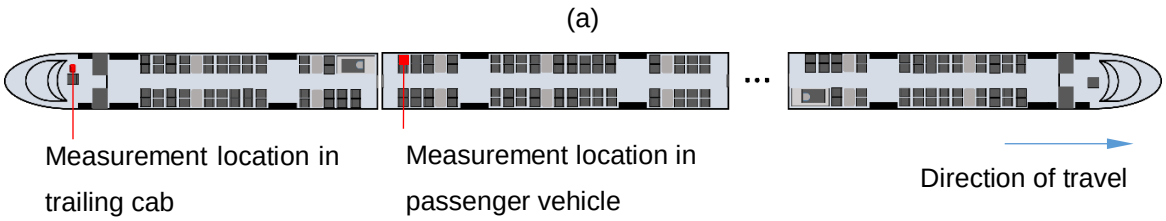

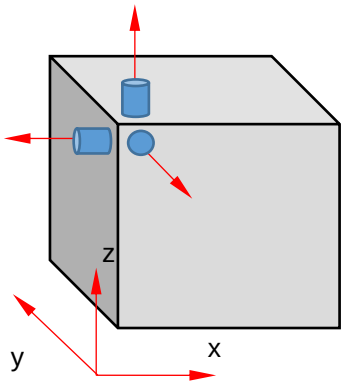

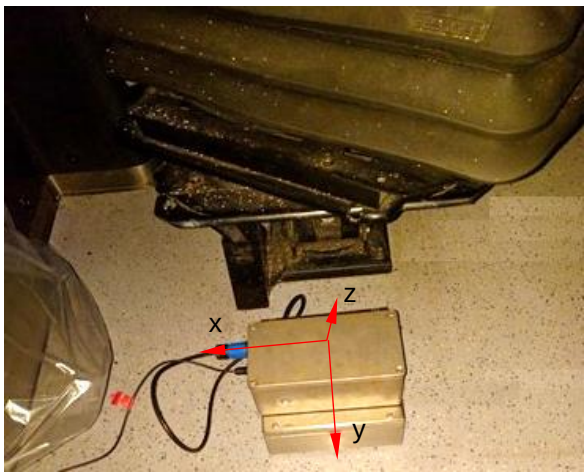

Figure 1 (a) Location of vibration measurements in a passenger train and in the trailing cab. (b) Vibration measurements in the passenger train showing locations of the accelerometers. (c) Positions of

accelerometers on the mounting block in the passenger train. (d) Position of the IMU mounted on the floor of the trailing cab.

Measurements of vibration were made at the seat, backrest and feet in accordance with ISO 2631-1[3] (Figures 1b and 1c). An aluminium block (15 cm x 15 cm x 15 cm, 6.23 kg) was placed on the carpet on the floor by the subject's feet. In laboratory tests it was determined that this block resting on a similar carpet can be considered to move rigidly with the floor at frequencies up to about 30 Hz. Three piezo-electric accelerometers were mounted at the top corner of the block to measure accelerations in the three translational axes (see Figure 1c). Accelerations in the three translational axes at the seat pan and backrest were measured by two SIT-pads containing tri-axial accelerometers. The vibration signals were acquired at a rate of 4096 samples per second, filtered with a low-pass filter at 100 Hz, and later resampled at 256 samples per second. GPS data were also recorded every 1 second. The DC components of acceleration were not measured because the sensors are piezo-electric.

Additionally, measurements in six axes were made using an inertial measurement unit (IMU) on the floor of the trailing cab (about 20 cm to the left of the longitudinal centre line, see Figure 1d) on the same 5 km section of track on a different occasion. The IMU contained a tri-axial accelerometer and three gyroscopes. These measurements covered the frequency range down to DC.

2.2 Measured track geometry

The geometry of the chosen 5-km section of track is shown in Figure 2. Two sources of track geometry data were used. First, the vertical and lateral irregularities on each rail have been obtained from routine track recording coach measurements. As is standard practice, these were high-pass filtered at a cut-off wavelength of 35 m and sampled at 0.4-m intervals. Second, the nominal alignment of the route has been obtained in terms of the gradients, the curvature, and the cant. From nominal information for vertical curves, the vertical long wavelength alignment was reconstructed and then sampled at 0.2-m intervals. To avoid sharp discontinuities in the rate of change of vertical curvature as well as lateral curvature, these profiles have been smoothed by applying a model of a static beam on an elastic foundation above the nominal profile. The beam was assigned the properties of a typical rail. The two sets of data for the vertical alignment and irregularities were combined and employed as relative vertical displacements between each wheel and the rail in a 'moving irregularity' model [30].

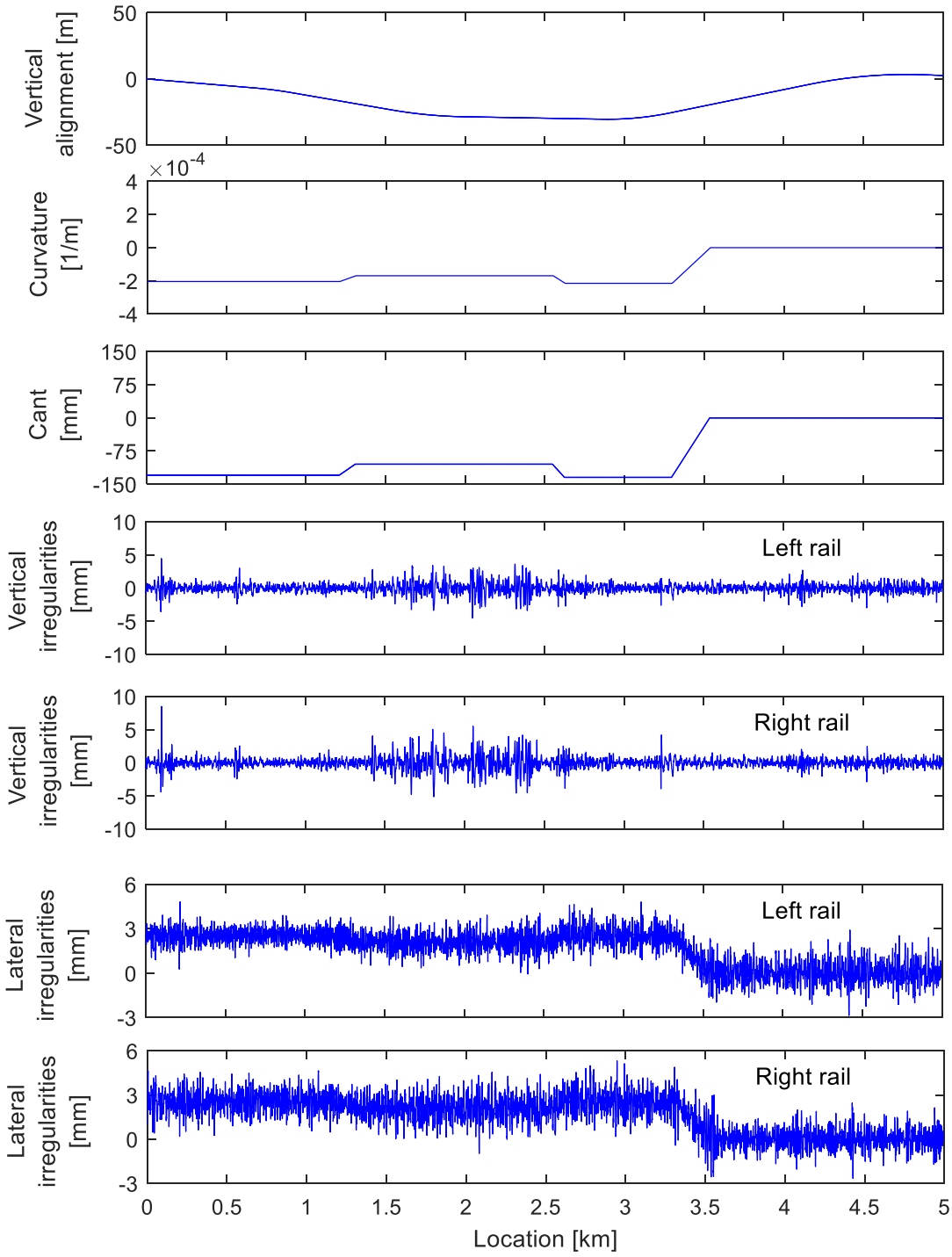

Figure 2 Components of track geometry including vertical alignment, curvature, cant, and vertical and lateral irregularities.

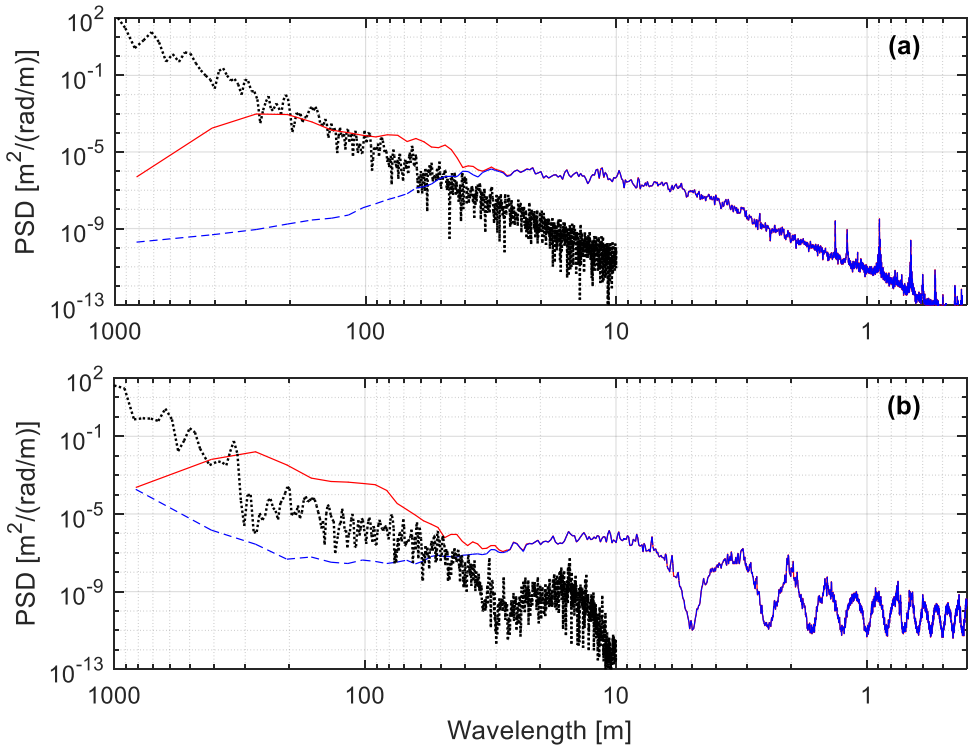

Figure 3 Comparison of measured alignment and irregularity and the extended vertical irregularity in vertical direction (a) and lateral direction (b): ····· measured alignment; – – – measured irregularity of left rail; —— extended irregularity.

The spectra of the separate inputs are shown in Figure 3. The spectrum of the vertical irregularities falls at wavelengths longer than 35 m due to the high-pass filtering. There is a gap between wavelengths of 35 m and 300 m which neither the vertical alignment nor the measured vertical irregularities cover. There is a similar gap between the lateral irregularities and the equivalent lateral alignment. Dips in the spectrum of the lateral irregularities may be attributed to the wheelbase distance of the measuring vehicle (approximately 2.5 m). The frequencies corresponding to different wavelengths are summarised in Table 1.

Table 1 Summary of frequencies corresponding to different wavelengths at different speeds.

Speed (km/h)	Frequency (Hz)			
	0.4	1.3	12	100
	Wavelength (m)			
200	140	43	4.6	0.56
300	210	64	6.9	0.83
400	280	85	9.3	1.11

The lateral long wavelength alignment is introduced in the vehicle model in terms of curvature and cant, rather than displacement. The spectrum of equivalent lateral alignment shown in Figure 3 has therefore been determined by running the model (described below) first with only the curvature and the cant of the track, and then with a straight track containing a certain level of lateral irregularity. The spectrum of the lateral irregularity was then scaled by the ratio of the spectra of the lateral accelerations of the car body between these two calculations to obtain the spectrum of the equivalent lateral alignment.

2.3 Extended track geometry spectrum

An extended track geometry spectrum for the missing wavelength range between 35 m and approximately 300 m has been determined by using the data from the IMU; these are more reliable in this wavelength range than those obtained with the piezo-electric accelerometers.

To generate this spectrum, a notional sample of vertical irregularity was generated containing wavelengths between 35 and 300 m. The model described below was run and the vertical acceleration of the vehicle was compared with the IMU data. The sample irregularity spectrum was adjusted to give a good match. The same approach was applied to generate the lateral irregularity with wavelengths between 35 and 300 m, but an iterative process was required because of the nonlinearities in the lateral vehicle/track interaction. The combination of the original track geometry and this new track geometry covers the whole wavelength range of interest. This combined track geometry is called the ‘extended track geometry’ and is shown in Figure 3. As the bouncing mode of the car body was found to be around 1.3 Hz (see Table 2), below 1 Hz the response of the car body is mainly determined by the track geometry. Therefore the extended track geometry based on the IMU data are not sensitive to the details of the vehicle model and are independent of the calibration process carried out below.

3 Dynamic models

3.1 Vehicle model

A conventional three-dimensional multi-body vehicle model including a car body, two bogies, and four wheelsets as detailed in *Refs* 25, 26 is used in this study, as shown in Figure 4. The wheelsets are connected to the bogie frame via primary suspension elements in the vertical, lateral and longitudinal directions, each represented by linear Kelvin-Voigt elements. Any offsets between the line of action of the springs and dampers and the displacements of the wheelsets are neglected. The bogies are similarly connected to the car body by secondary suspensions in the same three directions at each side of the vehicle. The car body is modelled as a beam, considering the first three flexible modes for each of vertical bending, lateral bending (both represented as an Euler-Bernoulli beam), and torsion. It is assumed for simplicity that there is no coupling between these different directions. The vehicle model has a total of 31 degrees of freedom (dofs) for the rigid motions, and 9 dofs are used for the generalised coordinates associated with the flexible modes of the car body. The longitudinal dofs are not included in the model.

Although lateral bending and torsion modes are coupled, for simplicity this effect is neglected here. The main effect of this coupling would be to shift the corresponding natural frequencies. The natural frequencies of the first bending and torsion modes are in any case similar to those found in the literature (e.g. Ref 22). Higher order modes will be more affected by coupling between bending and torsion. This will affect the spectrum of responses but would not significantly affect the overall weighted acceleration.

The vertical motion of the track is represented by a single-degree-of-freedom model in contact with each wheel. The parameters of the track model were obtained by fitting the receptance reported in Ref 28 at frequencies up to 80 Hz. In the lateral direction the track is assumed to be rigid.

The normal wheel/rail contact force is calculated for each wheel using a linearized Hertz contact stiffness [30]. Creep forces between the wheel and the rail are calculated using the FASTSIM algorithm [31]. At each step of the vehicle dynamics simulation, the contact patch between the wheels and rails is updated using a look-up table containing contact parameters [26]. All the calculated motions have been low-pass filtered at 120 Hz and then resampled at 256 samples per second.

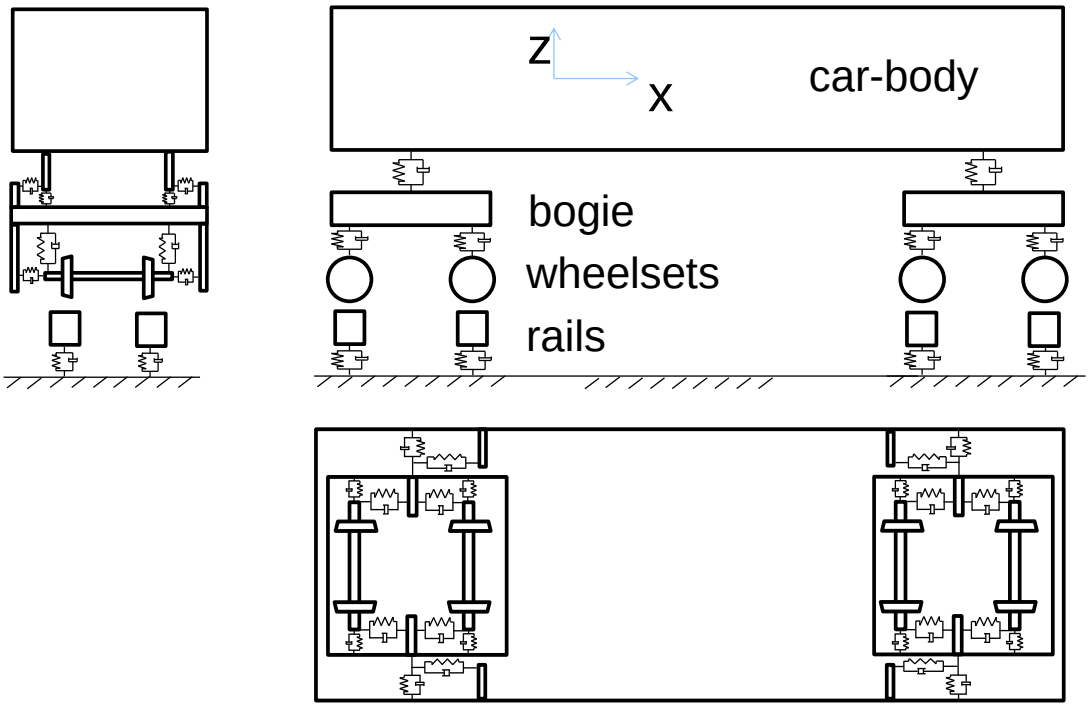

Figure 4 Dynamic model of the vehicle and the track.

3.2 Parameter identification using vibration measurements on a train

The floor accelerations measured by the two different measurement systems are compared in Figure 5. The translational accelerations generally show similar frequency dependence between 0.4 and 30 Hz. The remaining differences may be due to the different measurement locations in different vehicles.

In the absence of parameters for the test vehicles due to confidentiality reasons, the vehicle parameters were initially selected based on Refs 26 and 32. They were then adjusted to match the measured accelerations and such that the vibration modes occurred in a reasonable frequency range. The natural frequencies obtained from the updated model are consistent with Refs 13-14, 18-22 and are listed in Table 2. It should be noted that these vehicle model parameters are not claimed to represent the actual physical parameters of the vehicle. They are mainly intended to be a set of equivalent parameters that allow the interior vibration to be estimated from the track geometry. As such they are not unique, especially as the interior response is relatively insensitive to some parameters. The equivalent parameters are given in the Appendix.

Figure 5 also shows the unweighted accelerations at the floor obtained from the updated model. The floor vibration is well predicted apart from the roll. This is lower than the measured spectrum because

the irregularities in the extended track geometry for wavelengths between 35 and 300 m were the same for the two rails.

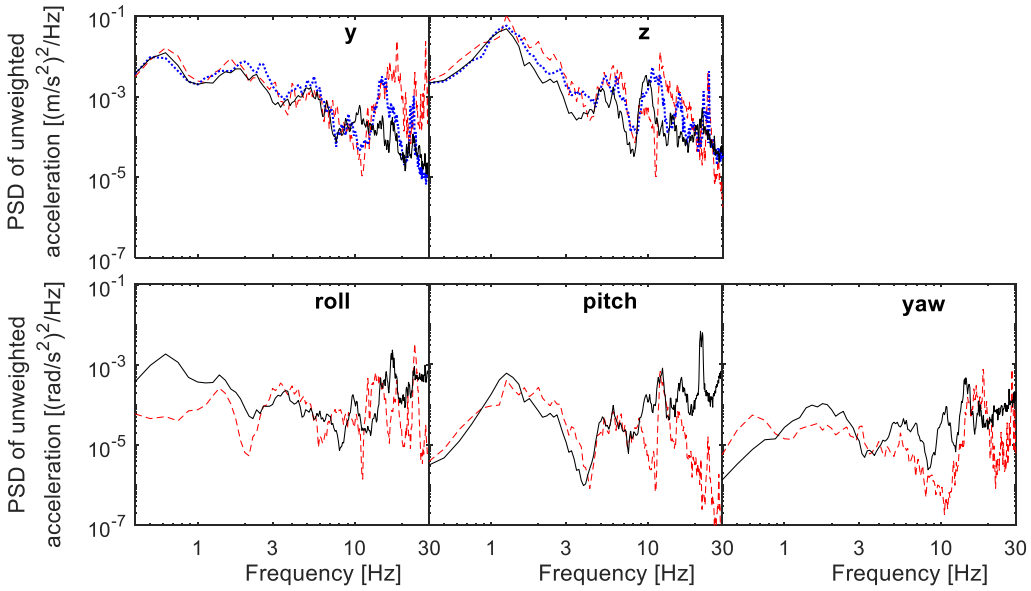

Figure 5 Power spectral density of unweighted accelerations at the floor: ····· measured at floor by seat position; —— measured using IMU; – – – modelled using extended track geometry. Train speed 210 km/h.

Table 2 Natural frequencies of the updated model.

	Mode shape	Frequency [Hz]
Car body	Bouncing	1.3
	Coupled roll and lateral motion: lower sway	1.5
	Coupled roll and lateral motion: upper sway	1.7
	Pitch	1.7
	Yaw	1.9
	Vertical bending: 1st order	11.7
	Vertical bending: 2nd order	32.3
	Vertical bending: 3rd order	63.3
	Lateral bending: 1st order	14.9
	Lateral bending: 2nd order	40.9
	Lateral bending: 3rd order	80.3
	Torsion: 1st order	12.1
	Torsion: 2nd order	24.2
	Torsion: 3rd order	36.3
Bogie	Bouncing	12.6
	Roll	17.7
	Pitch	19.2

3.3 Estimation of seat transmissibility

According to ISO 2631-1[3], to predict vibration discomfort requires knowledge of vibration at the seat pan and at the backrest as well as at the floor. To derive these for different speeds or track geometry, seat transmissibilities have been estimated from the measured accelerations. Figure 6 shows examples of the seat transmissibilities calculated from the operational data using the following transfer functions [33]:

$$H(f) = G_{ab}(f) / G_{aa}(f) \quad (1)$$

where $H(f)$ is the transmissibility; $G_{ab}(f)$ is the cross-spectral density function between a and b, $G_{aa}(f)$ is the power spectral density of a.

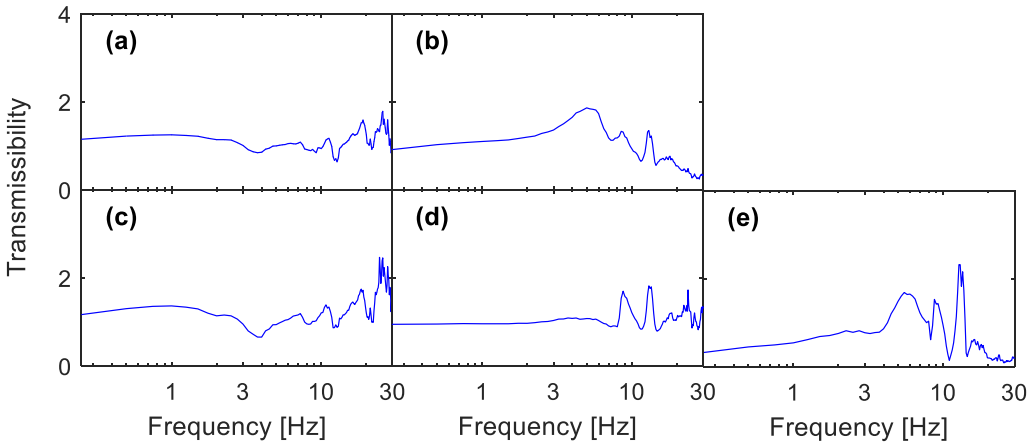

Figure 6 Seat transmissibilities used to estimate the vibration at the seat pan and the backrest: (a) from lateral floor acceleration to lateral seat acceleration; (b) from vertical floor acceleration to vertical seat acceleration; (c) from lateral floor acceleration to lateral backrest acceleration; (d) from vertical floor acceleration to vertical backrest acceleration; (e) from vertical floor acceleration to fore-and-aft backrest acceleration.

A seat is a multiple-input system in which motions in the various inputs can be partially coherent. In this study, it is assumed that where there is high coherence between one of the accelerations on the floor and on the seat, the transfer function between these locations can be used to represent the seat transmissibility. At frequencies between 0.5 and 20 Hz, the coherence was mostly close to unity for the various transfer functions shown in Figure 6. The coherence for other combinations of direction was generally less than 0.5.

Vertical and lateral accelerations at the seat pan and the backrest have been calculated from the vertical and lateral accelerations at the floor using the transfer functions given in Figure 6. The fore-and-aft backrest acceleration is approximated from the vertical floor acceleration (Figure 6e).

4 Evaluation of ride comfort

4.1 Comparison of vibration exposure between measurements and model

The overall weighted acceleration, which is a measure of vibration discomfort, has been determined here according to ISO 2631-1[3]. The standard gives ranges of values that are approximate indications of likely reactions as shown in Table 3. The rotational accelerations at the floor are used to approximate rotational accelerations at the seat pan. This simplification has limited influence on the overall weighted acceleration as the rotational vibrations generally contribute less to the overall vibration discomfort than translational vibration [34].

Table 3. Approximate indications of likely reactions to various magnitudes of overall total vibration in public transport (ISO 2631-1[3])

< 0.315 m/s^2	not uncomfortable
0.315 to 0.63 m/s^2	a little uncomfortable
0.5 to 1.0 m/s^2	fairly uncomfortable
0.8 to 1.6 m/s^2	uncomfortable
1.25 to 2.5 m/s^2	very uncomfortable
> 2 m/s^2	extremely uncomfortable

From the measurements at the passenger seat, the overall r.m.s. weighted acceleration was 0.358 m/s^2 when including the full frequency range up to 100 Hz, and 0.356 m/s^2 when applying a low-pass filter at 30 Hz to all the accelerations. The remaining comparisons are therefore limited to 30 Hz.

Figure 7 shows the weighted accelerations obtained from the measurements and the model. There is reasonable agreement for the vertical and lateral accelerations at the feet, seat pan and backrest and the fore-and-aft acceleration at the backrest at all frequencies. The prediction of these accelerations using the measured seat transmissibilities and floor accelerations from the model seems acceptable. Large discrepancies are present below 2 Hz for the roll motion because the irregularities in the extended track geometry for wavelengths between 35 and 300 m were the same for the two rails. For the vertical accelerations at the floor and at the backrest around 12 Hz there are some discrepancies between the predicted results and the measured ones, with a dip being present in the predicted spectrum around

11.2 Hz. This corresponds to a wavelength of 5.2 m, which is twice the wheelbase distance of 2.6 m. Nevertheless, despite these differences in the details of the spectrum, the general trend is predicted correctly, as is the overall weighted acceleration level (later shown in Figure 8). In the lateral and rotational directions there are discrepancies above 15 Hz mainly due to the simplicity of the car body beam model. Above 10 Hz, the modal density of the car body will be quite high[23] whereas only 9 modes are included here from the beam model. However, such discrepancies are expected to have little effect on the prediction of overall vibration discomfort, as shown later in Figure 8.

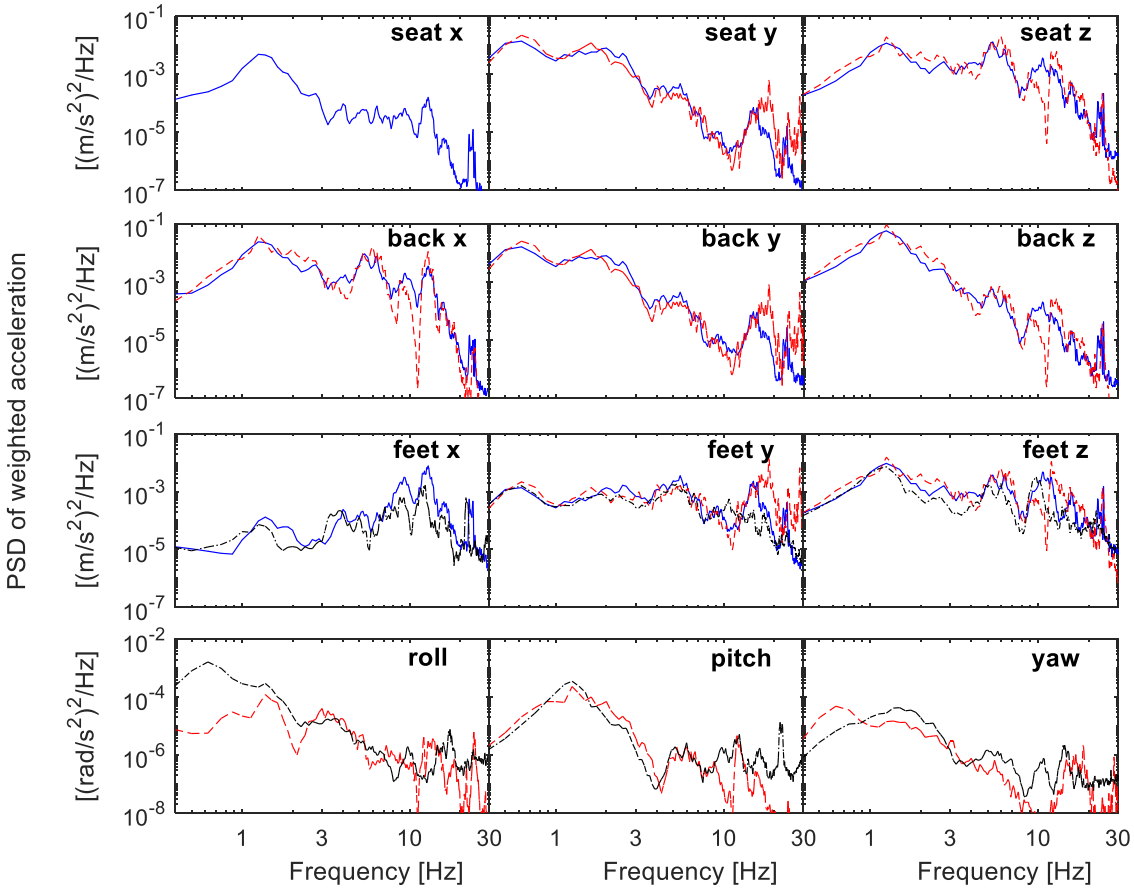

Figure 7 Comparison of power spectral densities of weighted accelerations (axis multiplying factors not applied) between measurements and the full model using extended track geometry: —— measured (seat position); – – – model; −·− IMU data (floor vibration only). Train speed 210 km/h.

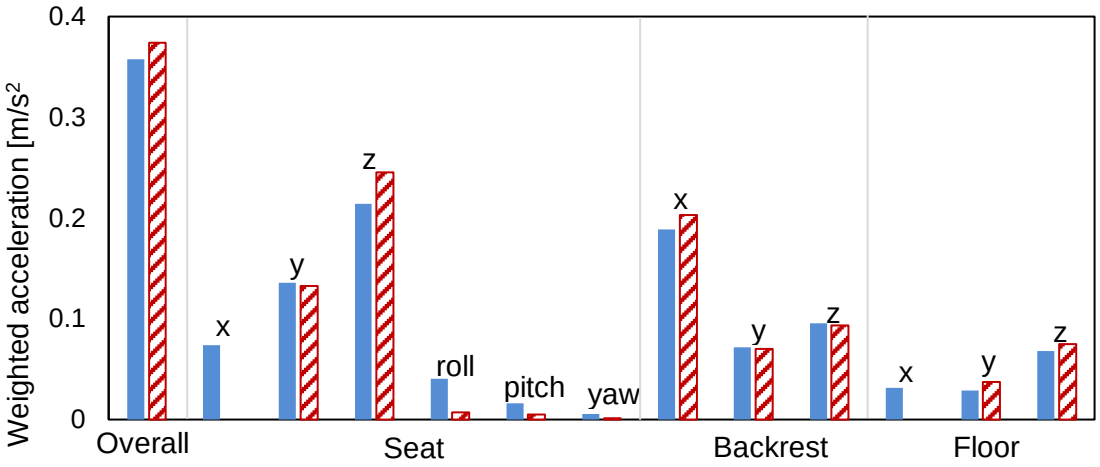

Figure 8 Overall weighted accelerations: ■ measured (passenger seat position); ▨ model. Rotational accelerations measured on the floor were used for seat. Unit of rotational acceleration changed into m/s^2 by multiplying by the axis factor as defined in ISO 2631-1[3]. Train speed 210 km/h.

The r.m.s. weighted accelerations for all locations and axes and their overall root-sum-of-squares [3] obtained from the measurements and the model are summarised in Figure 8. The vertical and lateral accelerations at the seat pan and the fore-and-aft acceleration at the backrest contribute most to the overall weighted vibration in the measurements, and this is well-predicted by the model. The rotational accelerations make little contribution to the overall weighted vibration, consistent with previous studies [34]. Based on the measured data, the overall r.m.s. weighted acceleration was 0.356 m/s^2 when including all 12 directions, and 0.349 m/s^2 when excluding the fore-and-aft acceleration at the seat pan and at the feet. Therefore the exclusion of the fore-and-aft accelerations at the floor and the seat pan has little influence on the overall weighted vibration.

4.2 Relative importance of components of track geometry on vibration discomfort at different speeds

Having established the applicability of the calibrated model, it is used to study the contributions of the different components of track geometry to ride comfort for different speeds. The model was run separately with each component of track geometry as well as with their combination at speeds between 200 and 400 km/h. It was ensured there was no hunting motion of the vehicle at any speed. The vibration discomfort is evaluated at the same seat position as before.

The overall weighted acceleration increases with increasing speed, by a factor of 2 between 200 and 300 km/h and by a factor of 3.5 between 200 and 400 km/h (Figure 9). At all speeds, the vibration caused by the vertical irregularities dominates the overall level, and that produced by the lateral

irregularities is the secondary contributor. The weighted acceleration produced by the other longer wavelength components of the geometry is much smaller.

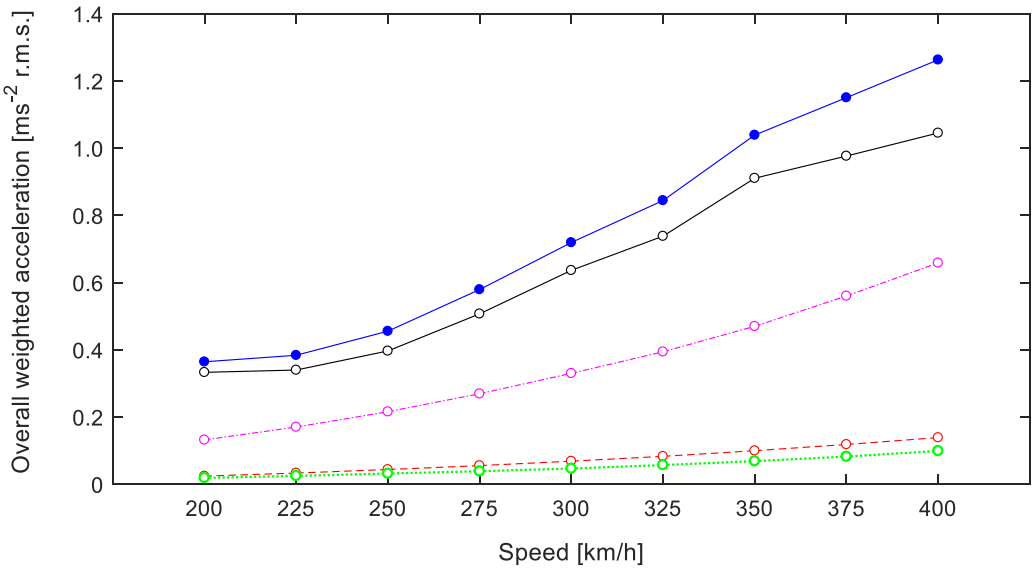

Figure 9 Contributions of different components of track geometry on overall weighted vibration obtained based on the extended track geometry: –●– combined track geometry; –o– vertical irregularities; –·o·– lateral irregularities; - o - vertical alignment; ····o··· horizontal curves.

4.3 Requirements on track wavelengths for high speeds

To refine the requirements for track geometry at high speeds, it is necessary to understand the discomfort produced by each wavelength component in the track at different speeds. Figure 10 shows contribution from each one-third octave wavelength band to the overall weighted vibration at different speeds. The dominant wavelengths are between 50 and 100 m for both the vertical and lateral irregularities, and between 5 and 12 m for the vertical irregularities. Both wavelength ranges appear as peaks in the overall weighted vibration.

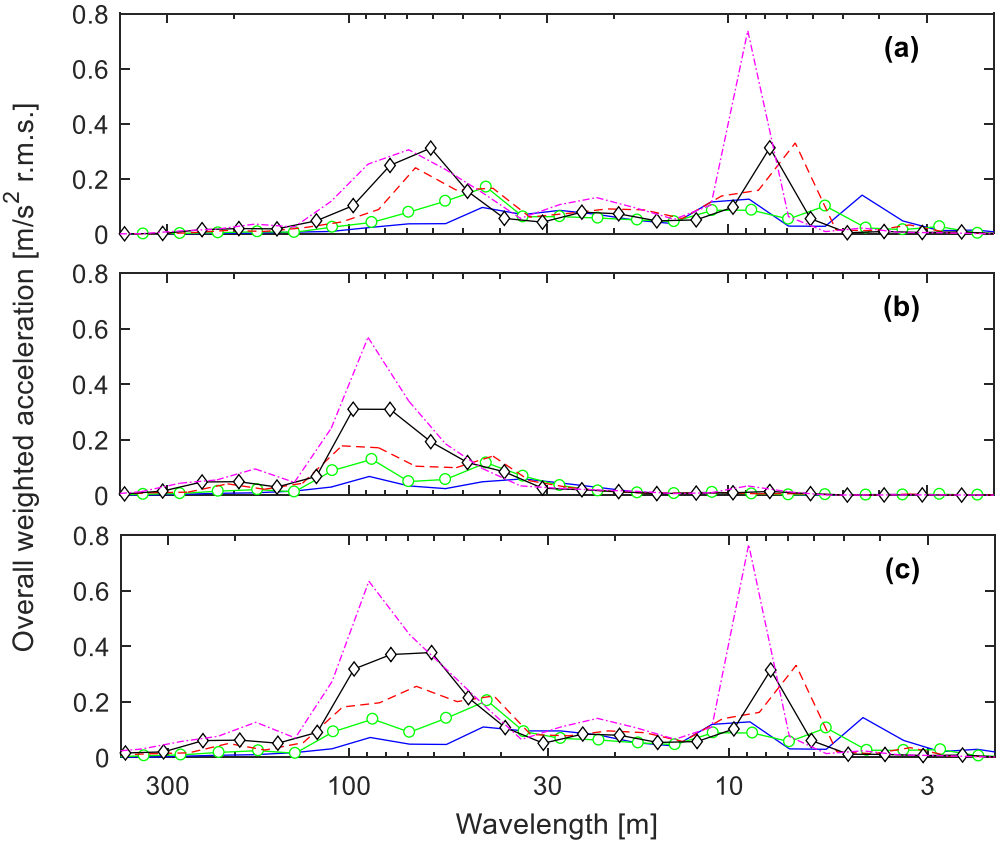

Figure 10 Contribution to overall weighted vibration by wavelengths between 3 and 300 m at different speeds obtained with (a) only vertical irregularity, (b) only lateral irregularity, and (c) all geometry components: —— 200 km/h; –o– 250 km/h; – – 300 km/h; –◊– 350 km/h; -·- 400 km/h. Plot in one-third octave frequency bands.

The peak response in the wavelength region between 100 and 50 m corresponds to a frequency of 1.3 Hz, which is the bounce mode of the car body on the suspension (see Table 2). The coupled roll and lateral modes at 1.5 and 1.7 Hz also occur in this frequency region. Therefore, to maintain a suitable level of overall weighted vibration at higher speeds, it is important that both the vertical and lateral irregularities with wavelengths between 50 and 100 m of a high-speed track should be controlled.

To predict the vibration discomfort of seated train passengers for speeds up to 400 km/h, the geometry of the track, particularly in the lateral direction, should be defined for wavelengths up to at least 150 m, whereas for speeds of 200 km/h and lower, wavelengths up to 60 m are sufficient. The omission of irregularities with wavelengths greater than 35 m, due to the common practice of applying a high-pass filter when measuring track irregularities, can lead to underestimates of the vibration severity by around 28% at 250 km/h and around 33% at 400 km/h.

Between 12 m and 5 m wavelength, the irregularities also show a greatly increased contribution to the overall weighted vibration as speed increases. The peak in this region corresponds to a frequency of 12 Hz, at which the first order vertical bending and torsional modes of the car body occur. If flexible modes are not included in the model, the weighted vibration would be underestimated by 6.1% at 200 km/h and 26% at 400 km/h. This is mainly due to the contributions of the first vertical bending mode and the first torsional mode of the car body.

4.4 Effect of the curvature and the cant of horizontal curves on vibration discomfort at different speeds

As seen in Figure 9, horizontal and vertical curves have only a small effect on ride comfort. To study the effect of curvature and cant of horizontal curves on vibration discomfort more explicitly, a single horizontal curve with transitions at the beginning and the end has been extracted from the track data. This track section contains a 500 m straight track followed by a 270 m linear transition into a curve. The steady curve lasts 1025 m and is then followed by a 270 m run-off transition. Five different values of radius (9000, 6000, 4500, 3600 and 3000 m) and of cant (70, 105, 140, 175, 210 mm) have been used for the curve. The radius of 4500 m with 140 mm cant is the current design of the track. The model has been run at five speeds between 200 and 400 km/h. No other irregularities in the vertical or lateral direction are included.

Figure 11 shows the overall weighted acceleration. For each curve radius, the overall weighted acceleration increases with increasing cant, irrespective of whether there is cant deficiency or excess. At speeds less than 350 km/h, the increase of overall weighted vibration with increasing cant is similar for all the radii, indicating that the motion of the car body due to the change of height difference between the two rails dominates. At higher speeds, the component $a_c \cos\theta$ (a_c is the centripetal acceleration in global coordinates and θ is the roll angle of the car body) increases and is great enough to contribute to the overall weighted vibration, especially with a small cant at a small radius (e.g. cant 70 mm and radius 3000 m). Nevertheless, in all cases the overall weighted acceleration remains much smaller than the component due to vertical and lateral irregularities, Figure 9.

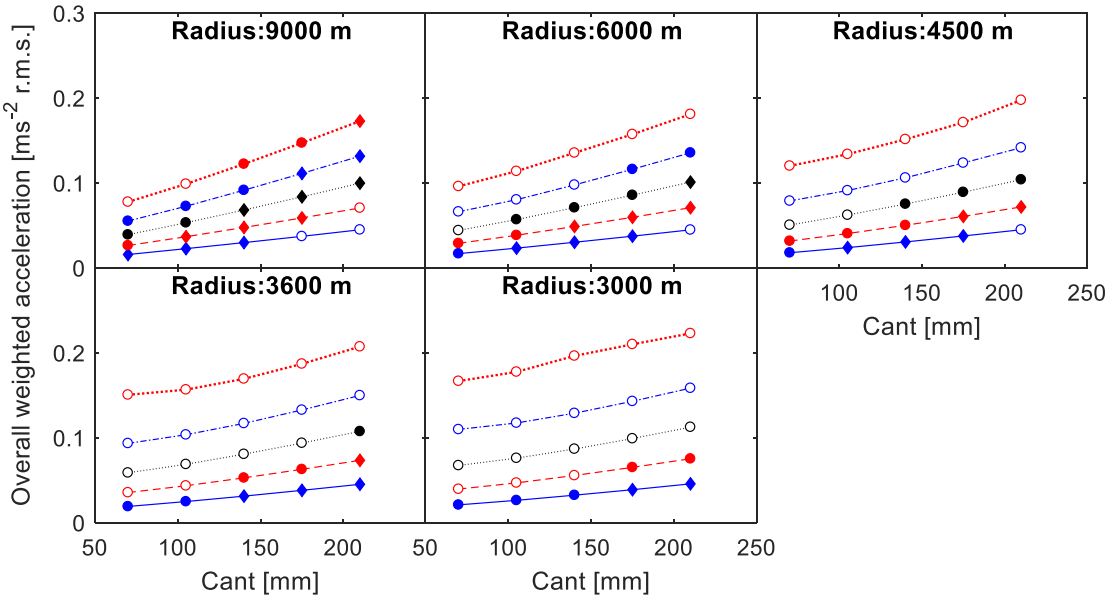

Figure 11 Effect of cant on overall weighted vibration with different lateral radii and speeds. —— 200 km/h; – – – 250 km/h; ····· 300 km/h; –·–· 350 km/h; ····· 400 km/h; solid diamond: cant excess less than 100 mm; solid circle: cant deficiency less than 100 mm; circle: others.

4.5 Effect of curvature of vertical curves on vibration discomfort with different speeds

To investigate the influence of vertical curves, a single vertical curve between two straight tracks was used. The straight parts are 500 m in length, and the vertical curve has a length of 444 m. As before, the geometry was smoothened by overlaying a beam-on-elastic-foundation model. No lateral curvature or cant was included and the track was otherwise smooth. The model has been run with five different radii (8, 12, 16, 20, and 24 km) and the same five different speeds.

Figure 12 shows the overall weighted acceleration as a function of vertical curvature. At each speed, with increasing vertical curvature the overall weighted vibration increases almost linearly. Again these weighted accelerations are much smaller than those due to vertical and lateral irregularities.

Although the horizontal and vertical curves have only a limited effect on vibration discomfort, they will have more significant effects on postural stability [35], motion sickness [36] and aspects of safety and maintenance [37]. However, these aspects are not considered in the current study.

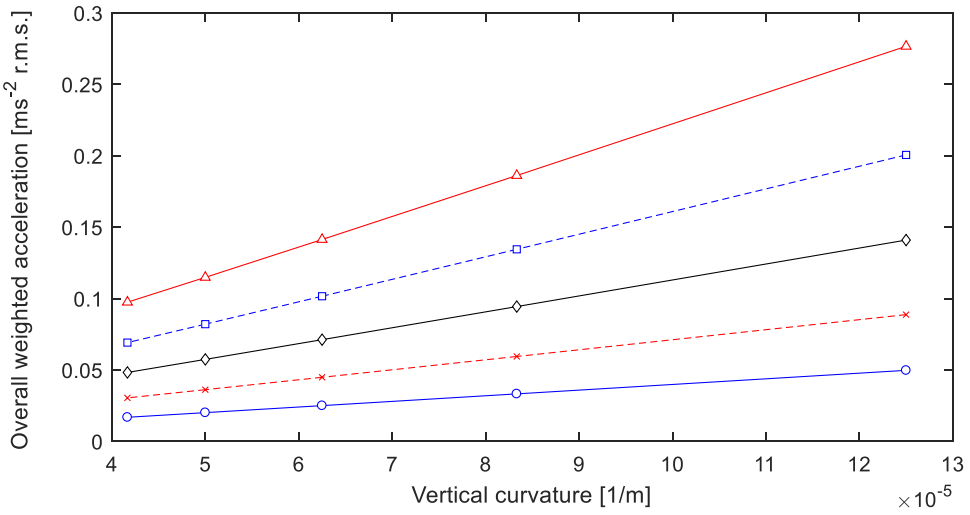

Figure 12 Effect of vertical curvature on overall weighted vibration at different speeds: –o– 200 km/h; – x – 250 km/h; –◊– 300 km/h; - -□- - 350 km/h; –△– 400 km/h.

5 Conclusions

An investigation is presented into the combined effect of speed and track geometry on vibration discomfort in high-speed trains. Railway vehicle dynamic models are used with the measured geometry of a section of high-speed track as an input. The models have been calibrated with vibration measurements carried out in a train running over this section of track and then applied to predict vibration discomfort at increased speeds.

The vibration discomfort of seated train passengers for speeds up to 400 km/h is affected by the geometry of the track, particularly in the lateral direction, with wavelengths up to at least 150 m, whereas for speeds of 200 km/h and lower, wavelengths up to 60 m are sufficient. The omission of irregularities with wavelengths greater than 35 m, due to the common practice of applying a high-pass filter when measuring track irregularities, can lead to underestimates of the vibration severity by around 28% at 250 km/h and around 33% at 400 km/h. If flexible modes of the car body are not included, the weighted vibration is underestimated by 6.1% at 200 km/h and 26% at 400 km/h. This is mainly due to the contributions of the first vertical bending mode and the first torsional mode of the car body.

The vertical irregularities are the dominant cause of vibration discomfort, although as speed increases the lateral irregularities also become important. The overall weighted acceleration increases by a factor of 2 between 200 and 300 km/h and by a factor of 3.5 between 200 and 400 km/h.

To maintain acceptable vibration discomfort as speed increases, the lateral and vertical irregularities of a high-speed track at wavelengths 50-100 m exciting the rigid modes of the car body, typically between 1 and 2 Hz, need to be controlled. Moreover, the vertical irregularities with wavelengths in the range 5-12 m, which excite the fundamental flexible mode of the car body around 10-15 Hz, require control.

All data published in this paper are openly available from the University of Southampton repository at https://doi.org/10.5258/SOTON/D1008.

Acknowledgements

The work was funded by the Engineering and Physical Sciences Research Council (EPSRC) through the research grants Track Systems for High Speed Railways: Getting It Right (EP/K03765X) and Track to the Future (EP/M025276). The authors are grateful for the assistance of Dr. David Milne from the University of Southampton and Dr. Paul Weston from the University of Birmingham.

Declaration of Conflicting Interests

The Authors declare that there is no conflict of interest.

Appendix

Table A1 Parameters of equivalent vehicle model

Parameter	Value	Unit
Mass of car body	35600	kg
Mass of bogie	2190	kg
Mass of wheelset	1530	kg
Roll moment of inertia of car body	39500	kgm^2
Pitch moment of inertia of car body	1.07×10^6	kgm^2
Yaw moment of inertia of car body	1.53×10^6	kgm^2
Roll moment of inertia of bogie	1460	kgm^2
Pitch moment of inertia of bogie	1460	kgm^2
Yaw moment of inertia of bogie	2740	kgm^2
Roll moment of inertia of wheelset	815	kgm^2
Yaw moment of inertia of wheelset	815	kgm^2
Total length of car body	20	m
Half longitudinal distance between bogie centres	7.1	m
Half longitudinal distance between axles of two wheelsets	1.3	m
Half lateral distance between primary springs and dampers	1.0	m
Half lateral distance between secondary springs and dampers	1.2	m
Vertical distance from the centre of gravity of each wheelset to that of the car body	1.19	m
Vertical distance from the centre of gravity of each wheelset to that of a bogie	0.068	m
Half track gauge	0.75	m
Nominal rolling radius of wheelset	0.42	m
Stiffness of primary longitudinal spring	21.5	MN/m
Stiffness of primary lateral spring	200	MN/m
Stiffness of primary vertical spring	3.15	MN/m
Stiffness of primary longitudinal damper	20	kNs/m

Stiffness of primary lateral damper	20	kNs/m
Stiffness of primary vertical damper	5.0	kNs/m
Stiffness of secondary longitudinal spring	8.0	MN/m
Stiffness of secondary lateral spring	1.0	MN/m
Stiffness of secondary vertical spring	0.605	MN/m
Damping of secondary longitudinal damper	1.3	kNs/m
Damping of secondary lateral damper	64	kNs/m
Damping of secondary vertical damper	26	kNs/m
Bending stiffness of beam for vertical bending	3.08	MNm^2
Bending stiffness of beam for lateral bending	4.95	MNm^2
Torsional stiffness of beam	450	MNm^2
Mass per unit length	1780	kg/m
Torsional inertia	1.93	kgm
Damping coefficients for vertical bending*	0.001	
Damping coefficients for lateral bending*	0.001	
Damping coefficients for torsion*	0.0001	
Effective stiffness of rail	99	MN/m
Effective damping of rail	200	kNs/m
Effective mass of rail	300	kg
Coulomb friction coefficient	0.3	
Hertzian contact stiffness	1.30×10^9	N/m

*Stiffness proportional coefficient of Rayleigh damping

References

1. Smith RA and Zhou J. Background of recent developments of passenger railways in China, the UK and other European countries. Journal of Zhejiang University-Science A (Applied Physics & Engineering) 2014; 15: 925-935.

2. BS 6841:1987. Measurement and evaluation of human exposure to whole-body mechanical vibration and repeated shock.

3. ISO 2631-1:1997. Mechanical vibration and shock – Evaluation of human exposure to whole-body vibration – part 1: general requirements.

4. UIC Code 703:1989. Layout characteristics for lines used by fast passenger trains.

5. BS EN 13848-5: 2017. Railway applications – Track – Track geometry quality – part 5: geometric quality levels.

6. Tian GY, Gao JM, Zhai WM. Comparative analysis of track irregularity management standards for high-speed railways. Journal of the China Railway Society, 2015; 3: 64-71.

7. The Ministry of Railway of PRC. Ballast track repair rules of high-speed railway (temp). Beijing: China Railway Publishing House, 2013.

8. The Ministry of Railway of PRC. Ballastless track repair rules of high-speed railway (temp). Beijing: China Railway Publishing House, 2013.

9. EN 12299:2009. Railway applications – ride comfort for passengers – measurement and evaluation, 2009.

10. ISO 10056:2001. Mechanical vibration – measurement and analysis of whole-body vibration to which passengers and crew are exposed in railway vehicles.

11. ISO 2631-4:2001. Mechanical vibration and shock – evaluation of human exposure to whole-body vibration – part 4: guidelines for the evaluation of the effects of vibration and rotational motion on passenger and crew comfort in fixed–guideway transport systems.

12. UIC Code 513:1994. Guidelines for evaluating passenger comfort in relation to vibration in railway vehicles.

13. Sun W, Zhou J, Thompson DJ, Gong D. Vertical random vibration analysis of vehicle–track coupled system using Green's function method. Vehicle System Dynamics 2014; 52: 362 – 389.

14. Tomioka T, Takigami T, Suzuki T. Numerical analysis of three-dimensional flexural vibration of railway vehicle car body. Vehicle System Dynamics 2006; 44: 272 – 285.

15. Kargarnovin MH, Younesian D, Thompson DJ, Jones C. Ride comfort of high-speed trains travelling over railway bridges. Vehicle System Dynamics 2005; 43: 173 – 199.

16. Cheng YC, Lee SY, Chen HH. Modeling and nonlinear hunting stability analysis of high-speed railway vehicle moving on curved tracks. Journal of Sound and Vibration 2009; 324: 139-160.

17. Zhou J, Goodall R, Ren L, Zhang H. Influences of car body vertical flexibility on ride quality of passenger railway vehicles. Proceedings of the Institution of Mechanical Engineers, Part F: Journal of Rail and Rapid Transit 2009; 223: 461 – 471.

18. Kumar V, Rastogi V, Pathak PM. Simulation for whole-body vibration to assess ride comfort of a low–medium speed railway vehicle. Simulation 2017; 93: 225 – 236.

19. Huang C, Zeng J, Luo G, Shi H, Numerical and experimental studies on the car body flexible vibration reduction due to the effect of car body-mounted equipment. Proceedings of the Institution of Mechanical Engineers, Part F: Journal of Rail and Rapid Transit 2018; 232(1): 103–120.

20. Iwnicki S. Manchester Benchmarks for Rail Vehicle Simulation. Vehicle System Dynamics 1999; 31.

21. Iwnicki S. Handbook of railway vehicle dynamics. CRC Press, 2006.

22. Zheng X, Hao Z, Wang X, Mao J. A full-spectrum analysis of high-speed train interior noise under multi-physical-field coupling excitations. Mechanical Systems and Signal Processing 2016; 75: 525 – 543.

23. Diana G, Cheli F, Collina A, Corradi R, Melzi S. The development of a numerical model for railway vehicles comfort assessment through comparison with experimental measurements, Vehicle System Dynamics 2002; 38: 165 – 183.

24. Howarth HVC and Griffin MJ. A comparison of standardised methods of evaluating rail vehicle vibration with respect to passenger discomfort. The 39th United Kingdom Conference on Human Response to Vibration, Ludlow, Shropshire, England, 15-17 September 2004.

25. Wickens AH. Fundamentals of Rail Vehicle Dynamics – Guidance and Stability. Swets & Zeitlinger Publishers, Lisse, 2003.

26. Huang Z. Theoretical Modelling of Railway Curve Squeal. PhD thesis, University of Southampton, UK, 2007.

27. Universal Mechanism Software, Simulation of rail vehicle dynamics, User's Manual, 2016.

28. Thompson DJ and Vincent N. Track dynamic behaviour at high frequencies. Part 1: theoretical models and laboratory measurements. Vehicle System Dynamics 1995; 24: 86 – 99.

29. Graa M, Nejlaoui M, Houidi A, Affi Z, Romdhane L. Development of a reduced dynamic model for comfort evaluation of rail vehicle systems. Proceedings of the Institution of Mechanical Engineers, Part K: Journal of Multi-Body Dynamics 2016; 230(4): 489–504.

30. Thompson DJ. Railway Noise and Vibration: Mechanisms, Modelling and Means of Control, Elsevier Science, Oxford, UK, 2008.

31. Kalker JJ. A fast algorithm for the simplified theory of rolling contact, Vehicle System Dynamics 1982; 11: 1 – 13.

32. Iwnicki S. Manchester benchmarks for rail vehicle simulation. Vehicle System Dynamics 1998; 30: 295-313.

33. Shin K, Hammond J. Fundamentals of Signal Processing for Sound and Vibration Engineers. Wiley-Blackwell, 2008.

34. Griffin MJ. Handbook of human vibration. Elsevier Academic Press, UK, 1990.

35. Sari HM and Griffin MJ. Postural stability when walking: Effect of the frequency and magnitude of lateral oscillatory motion. Applied Ergonomics 2014; 45: 293 – 299.

36. Donohew BE and Griffin MJ. Low frequency motions and motion sickness on a tilting train, Proceedings of the Institution of Mechanical Engineers, Part F: Journal of Rail and Rapid Transit 2007; 221: 125 – 133.

37. Choi IY, Um JH, Lee JS, Choi HH. The influence of track irregularities on the running behavior of high-speed trains. Proceedings of the Institution of Mechanical Engineers, Part F: Journal of Rail and Rapid Transit 2013; 227(1): 94–102.